Geophysical Research Letters

RESEARCH LETTER
10.1029/2019GL085329

South Asian Summer Monsoon Response to Aerosol-Forced Sea Surface Temperatures

Xiaoqiong Li[1,2], Mingfang Ting[1], Yujia You[1,2], Dong-Eun Lee[1,3], Daniel M. Westervelt[1,4], and Yi Ming[5]

[1]Lamont-Doherty Earth Observatory, Columbia University, Palisades, NY, USA, [2]Department of Earth and Environmental Sciences, Columbia University, Palisades, NY, USA, [3]Department of Marine Environmental Sciences, ChungNam National University, Daejeon, South Korea, [4]Goddard Institute for Space Studies, New York, NY, USA, [5]NOAA/Geophysical Fluid Dynamics Laboratory, Princeton, NJ, USA

Abstract Climate models suggest that anthropogenic aerosol-induced drying dominates the historical rainfall changes over the heavily populated South Asian monsoon region. The regional response depends on both the aerosol fast radiative effect and the slow process through sea surface temperature (SST) cooling. Two atmospheric general circulation models, NCAR-CAM5 and GFDL-AM3, are used to investigate the monsoon response to prescribed aerosol-forced SSTs. The total SST is separated into uniform cooling and a spatially varying component characterized by interhemispheric asymmetry. The monsoon rainfall is predominantly controlled by the nonuniform SSTs, in the local Indian Ocean, South, and East China Seas (IO-CSs). The reduced meridional SST gradient in the IO-CSs leads to weakened monsoon circulation, which drives a north-south dipole rainfall change. The latitudinal location of the dipole shows model dependence due to differences in local SSTs and their meridional gradient, which determines the latitudinal location of the meridional overturning circulation responses.

Plain Language Summary South Asian monsoon rainfall is an important part of the region's economy as it affects the agriculture and water supply in this densely populated region. Anomalously weak monsoon rainfall can lead to catastrophic crop failures and famine. Recent increases in aerosol emission not only caused severe air pollution problems in the region, but also led to monsoon circulation and rainfall changes. Previous studies have shown that aerosols can lead to drying in a region due to interaction with radiation and clouds. Additionally, the northern hemisphere centric aerosol emission led sea surface temperatures to cool more in northern than southern hemispheres. This sea surface temperature mediated responses to aerosol can play an important role in the South Asian monsoon response to aerosols. In this study, we demonstrate that this effect is mainly through the north-south temperature gradient in the Indian Ocean, South, and East China Seas, which leads to atmospheric circulation that weakens the monsoon overturning and drying in South Asia. However, the exact latitudes of this drying tend to be highly model-dependent due to different sea surface temperatures in the local ocean basins.

Key Points:
- Predominant impact of aerosol-forced sea surface temperatures on South Asian monsoon is the local spatially nonuniform part
- Large intermodel differences in monsoon responses are due to regional aerosol-forced SST differences
- Dynamical mechanisms dominate South Asian drying due to SST-mediated aerosol forcing

Supporting Information:
- Supporting Information S1

Correspondence to:
M. Ting,
ting@ldeo.columbia.edu

Citation:
Li, X., Ting, M., You, Y., Lee, D.-E., Westervelt, D. M., & Ming, Y. (2020). South Asian summer monsoon response to aerosol-forced sea surface temperatures. *Geophysical Research Letters*, *47*, e2019GL085329. https://doi.org/10.1029/2019GL085329

Received 9 SEP 2019
Accepted 10 DEC 2019
Accepted article online 3 JAN 2020

1. Introduction

As the two most important anthropogenic forcing agents, greenhouse gases (GHGs) and aerosols often lead to distinctly different changes in the climate system. The opposing radiative forcing as well as the contrasting effects on the surface temperature results in different responses in atmospheric circulation and global and regional hydroclimate (e.g., Singh, 2016 ; Wang et al., 2016; Xie et al., 2013). Aerosols offset the global warming signal imposed by GHGs while inducing a hemispheric temperature contrast due to the spatial inhomogeneity of aerosol emissions over the globe (Bollasina et al., 2011; Lau & Kim, 2017; Li et al., 2018; Westervelt et al., 2017; Westervelt et al., 2018). In the Asian monsoon region, in contrast to the surface temperature response which is governed by GHGs, climate models suggest that historical rainfall changes are dominated by aerosol-induced drying trend in the twentieth century, as shown in Li et al. (2015) using Coupled Model Intercomparison Project-Phase 5 (CMIP5) models. However, the regional response of atmospheric circulation and rainfall to global and regional anthropogenic aerosol forcing is not yet well understood and constrained, particularly for processes related to ocean-atmosphere interactions (Turner & Annamalai, 2012; Xie et al., 2015).

The climate response to external forcing agents involves two components on different time scales: (1) the fast adjustment due to radiative effects as well as the influence on clouds and the land surface and (2) the slow

response due to changes in sea surface temperature (SST) (Allen & Ingram, 2002; Andrews et al., 2009; He & Soden, 2015; Liu et al., 2018; Samset et al., 2016). The fast adjustment of precipitation and atmospheric circulation to GHG and aerosol forcing and the possible compensating effects between the fast and slow responses have been investigated in many previous studies (e.g., Bony et al., 2013; Li et al., 2018; Li & Ting, 2017; Liu et al., 2018; Richardson et al., 2016; Shaw & Voigt, 2015; Wang et al., 2019). The slow response involving mediation through SSTs is also critically important for the atmospheric circulation and rainfall response in the tropics (e.g., Ma & Xie, 2013; Chadwick et al., 2013). Compared to the relatively homogeneous spatial distribution of well-mixed long-lived GHGs, aerosol radiative forcing concentrates over the northern hemisphere continents and exhibits pronounced hemispheric asymmetry (Hill et al., 2015; Shindell et al., 2013). On a global scale, the aerosol-associated hemispheric difference of thermal forcing and meridional temperature gradient renders more northward energy transports and results in a southward shift of the intertropical convergence zone (Allen, 2015; Kang et al., 2008; Ming & Ramaswamy, 2009, 2011; Seo et al., 2014; Westervelt et al., 2017).

Previous studies highlighted the importance of improving the understanding of the various physical pathways by which the external forcing agents impact atmospheric circulation and precipitation for better constraining uncertainties. In both CMIP3/5 models, the SST spatial pattern provides the largest source of uncertainty and intermodel spread in precipitation and atmospheric circulation changes (Chen & Zhou, 2015; Kent et al., 2015; Ma & Xie, 2013). Moreover, while most studies address global-scale slow response in precipitation and circulation (e.g., He et al., 2014; Hill et al., 2015; Ma & Xie, 2013), fewer studies have focused on regional and local scales, especially the heavily populated Asian monsoon region (Bollasina et al., 2011; Chadwick et al., 2013; Ganguly et al., 2012; Kim et al., 2016; Li & Ting, 2015, 2017; Li et al., 2018). For GHGs, Li and Ting (2017) showed that uniform SST warming induces a larger model spread in summer monsoon rainfall and circulation response over land compared to the fast adjustment. For aerosols, Li et al. (2018) suggested that while the fast adjustment dominates over eastern China and northern India, the slow response is important in altering the meridional circulation over the oceanic regions. However, Li et al. (2018) did not examine the mechanisms driving the SST-related slow responses.

The motivation of this study is to gain a better mechanistic understanding of the slow responses of summer monsoon circulation and rainfall to historical aerosol-induced SST changes. The goal is to identify the relative importance of uniform versus spatially varying SST changes, and local versus remote SSTs in driving the monsoon response. A suite of idealized experiments using two atmospheric general circulation models (AGCMs) is designed to delineate the effects of different SST forcing on the South Asian summer monsoon, as well as to determine the model dependence and uncertainty of the responses.

2. Methods

2.1. AGCMs

We use two AGCMs to perform idealized experiments: the National Center for Atmospheric Research (NCAR) Community Atmosphere Model version 5.3 (CAM5) and the Geophysical Fluid Dynamics Laboratory Atmospheric Model version 3 (GFDL-AM3). CAM5 is the atmospheric component of the Community Earth System Model (CESM) version 1.2.2.1 with 30 vertical levels, coupled to an interactive land model (CLM4), with f19 (1.9° latitude × 2.5° longitude) horizontal resolution. GFDL-AM3 is the atmospheric component of the coupled climate model version 3 (GFDL-CM3) with 48 vertical levels, coupled to the land model LM3. For GFDL-AM3, we use the C48 cubed-sphere horizontal grid with six faces of 48 grid cells along each edge (approximately a 2° × 2° resolution). Detailed descriptions of the two models including the dynamical core and physical parameterizations can be found in Neale et al. (2012) for CAM5 and Donner et al. (2011) for GFDL-AM3.

2.2. Experimental Design

We design prescribed SST experiments to examine the influence of different SST forcing on monsoon changes. For all experiments, aerosol emissions are fixed at year 1850 level, ensuring that the response is solely due to the change in the imposed SSTs. We use climatological SST and sea ice concentration of 1951–2000 from the HadISST data for the control experiment (SST_CTRL). We derive the total SST anomaly from the historical aerosol-only simulations of the respective fully coupled model (CESM-CAM5 and GFDL-CM3), calculated as the difference between period 1981–2005 and 1861–1885. For both models, the ensemble mean of the three

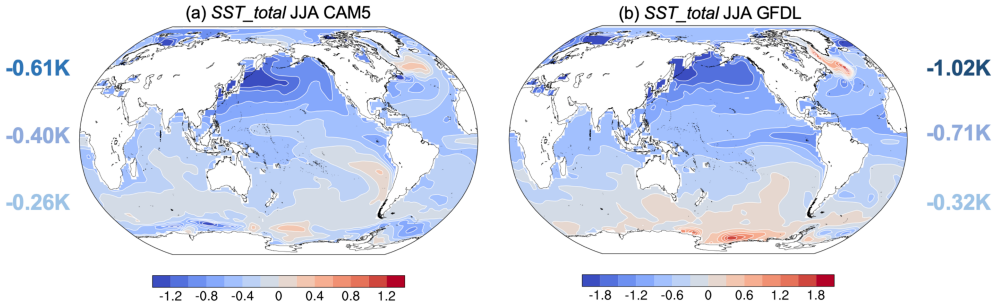

(c)

Experiment	Prescribed SST
CTRL	HadISST 1951-2000 climatology
SST_total	clim + total SST anomaly from CGCM aerosol-only simulation
SST_uni	clim + uniform cooling of tropical mean of total
SST_structured	clim + total - uni (global)
SST_structured_IO+SCS	clim + total - uni (Indian Ocean+South China Sea)

Figure 1. June–August (JJA) global sea surface temperature anomalies (difference between 1981–2005 and 1861–1885) in *SST_total* experiment of (a) CAM5 and (b) GFDL-AM3. Units are in °K. (c) List of experiments performed in this study. The numbers on the side of (a) and (b) represent Northern Hemisphere average (top), tropical (30°S–30°N) average (middle), and Southern Hemisphere average (bottom) values of SST in the respective model.

members of the aerosol-only simulations is used. This total SST anomaly (SST_total) is added to the SST_CTRL climatology. We then separate the total SST anomaly into two components: (1) the uniform cooling component (SST_uni), calculated as the annual mean of the tropical oceans (30°S–30°N) from the total, and (2) the spatially varying component, calculated as the difference between the total and the uniform cooling (SST_structure). This decomposition method follows Ma and Xie et al. (2013) using CAM3 and Hill et al. (2015) using GFDL-AM2.1. Although such a decomposition enables us to disentangle the role of uniform and structured SST changes, it does not necessarily separate the role of local from remote SST-driven responses. Hence, an additional experiment is conducted with the structured SSTA prescribed only in the Indian Ocean, South, and East China Seas region (SST_structure_IO-CSs, see supporting information Figure S1). All experiments are run for 60 years after an initial 1-year spin-up.

Figures 1a and 1b present the total SST anomaly derived from the fully coupled models and used in the corresponding AGCM experiments for June, July, and August (JJA) average. The JJA SSTA averaged for the Northern Hemisphere (NH), Southern Hemisphere (SH), and the tropics are also shown in Figure 1. The spatial SST asymmetry between the NH and SH bears a close resemblance between the two models with stronger cooling in the NH, especially over the midlatitude North Pacific. The spatial correlation between the two SSTA patterns is 0.73. Although similar in spatial pattern, GFDL-CM3 has a larger amplitude in the historical period, with the tropical-averaged (30°S to 30°N) SST changes of −0.71 K compared to −0.40 K in CAM5. The north-south interhemispheric SST difference is twice as strong in GFDL-CM3 as compared to CAM5 (−0.7 K versus −0.35 K). The hemispheric SST contrast is of comparable magnitude to the uniform cooling in both models. Model experimental details are listed in Figure 1c as a reference.

2.3. Moisture Budget Analysis

We analyze the atmospheric moisture budget to quantify physical processes driving changes in precipitation, following Li and Ting (2017), Li et al. (2018), and Seager and Henderson (2013). The moisture budget equation for steady state is as follows:

$$\overline{P}-\overline{E} = -\frac{1}{g\rho_w}\nabla\cdot\overline{\int_0^{p_s}\mathbf{u}q dp} \approx -\frac{1}{g\rho_w}\nabla\cdot\sum_{k=1}^{K}\overline{\mathbf{u}_k q_k p_k}, \quad (1)$$

where P is precipitation, E is evaporation, g is the gravitational acceleration, ρ_w is the density of water, p is

atmospheric pressure and p_s surface pressure, $\mathbf{u}$ is the horizontal wind vector, q is specific humidity, and k is the vertical level with a total of K (outputs for both models are interpolated to standard pressure levels, then integrated from 1,000 to 200 hPa with a total K = 10 levels), p is the pressure thickness. Overbars represent monthly mean values.

Using primes to denote departures from monthly means, the moisture flux convergence term can be separated into the mean moisture convergence (MC) and the submonthly transient eddies (TE)

$$\overline{P}-\overline{E}\approx-\frac{1}{g\rho_w}\nabla\cdot\sum_{k=1}^{K}\overline{\mathbf{u}}_k\overline{q}_k\overline{p_k}-\frac{1}{g\rho_w}\nabla\cdot\sum_{k=1}^{K}\overline{\mathbf{u}_k{}'q_k{}'}\,\overline{p_k}. \tag{2}$$

The contribution of the transient eddy component is small over the monsoon region (Li et al., 2018), thus we quantify the forced response using the mean MC term, and define

$$\delta\overline{\overline{(.)}}=\overline{\overline{(.)}}_F-\overline{\overline{(.)}}_C \tag{3}$$

to represent the difference between the forced (F) and control (C) experiments, where the second overbar denotes the 60-year mean. The change in the mean MC can be separated into a thermodynamic component due to changes in moisture (δTH), and a dynamic component due to changes in atmospheric circulation (δDY), as follows:

$$\begin{aligned}\delta\overline{\overline{MC}}&=\left(-\frac{1}{g\rho_w}\overline{\overline{\nabla\cdot\sum_{k=1}^{K}\overline{\mathbf{u}}_{k,F}\overline{q}_{k,F}\overline{\Delta p}_{k,F}}}\right)-\left(-\frac{1}{g\rho_w}\overline{\overline{\nabla\cdot\sum_{k=1}^{K}\overline{\mathbf{u}}_{k,C}\overline{q}_{k,C}\overline{\Delta p}_{k,C}}}\right)\\&\approx-\frac{1}{g\rho_w}\nabla\cdot\sum_{k=1}^{K}\overline{\overline{\mathbf{u}}}_{k,}\,C\delta\overline{\overline{q}}_k\overline{\overline{\Delta p}}_k-\frac{1}{g\rho_w}\nabla\cdot\sum_{k=1}^{K}\delta\overline{\overline{\mathbf{u}}}_k\overline{\overline{q}}_{k,C}\overline{\overline{\Delta p}}_k\\&=\delta\overline{\overline{TH}}+\delta\overline{\overline{DY}}.\end{aligned} \tag{4}$$

3. Results

The climatological difference between the forced and control experiment quantifies the slow response to the prescribed aerosol-induced SSTs. We concentrate on South Asia and adjacent oceans where the slow response over the Asian monsoon region is the most prominent (e.g., Li et al., 2018). Using the 60-year AGCM simulation, significant rainfall response above the atmospheric internal variability is detected. In both models, the spatial distribution of summertime (JJA) rainfall to the aerosol-induced total SST change is characterized by a meridional dipole across the equator (boxed regions in Figures 2a and 2d). While a strong similarity between the models is found in terms of the wetting tendency in the equatorial South Indian Ocean between 40°E and 100°E, the location of the drying tendency differs: CAM5 simulates a below-normal rainfall over the Indian subcontinent, Bay of Bengal, and South China Sea between 10°N and 25°N (Figure 2a), whereas GFDL-AM3 projects drying over the equatorial IO between 5°S and 10°N, with weak drying over the Indian subcontinent (Figure 2e). The results here are consistent with Li et al. (2018), who suggested that the slow response to aerosol through SST cooling is a dipole with sinking motion near the equator and rising motion over the Indian Ocean at about 10°S. Our results further suggest large differences in the exact location of this dipole pattern across different models.

The rainfall response to the aerosol-induced total SST is further divided into that due to uniform and spatially structured SST changes in Figures 2b–2c and 2f–2g for each model. Even though the uniform SST cooling is comparable in magnitude to the interhemispheric SST difference in both models (Figures 1a and 1b), the rainfall responses are dominated by the asymmetric interhemispheric SST changes. Furthermore, the rainfall responses to the global and local spatially structured SST are not significantly different (Figures 2c, 2d and 2g, 2h), indicating the predominant role played by the local SST in shaping the slow response of South Asian summer monsoon to aerosol forcing. A recent study (Wang et al., 2019) found that the global zonal mean SST, which contains a strong north-south gradient, is the dominant cause of the monsoon rainfall response, while the regional IO SST played a secondary role. The discrepancy between their results and Figure 2 is mainly due to the inclusion of the South and East China Seas (CSs) SST in our local

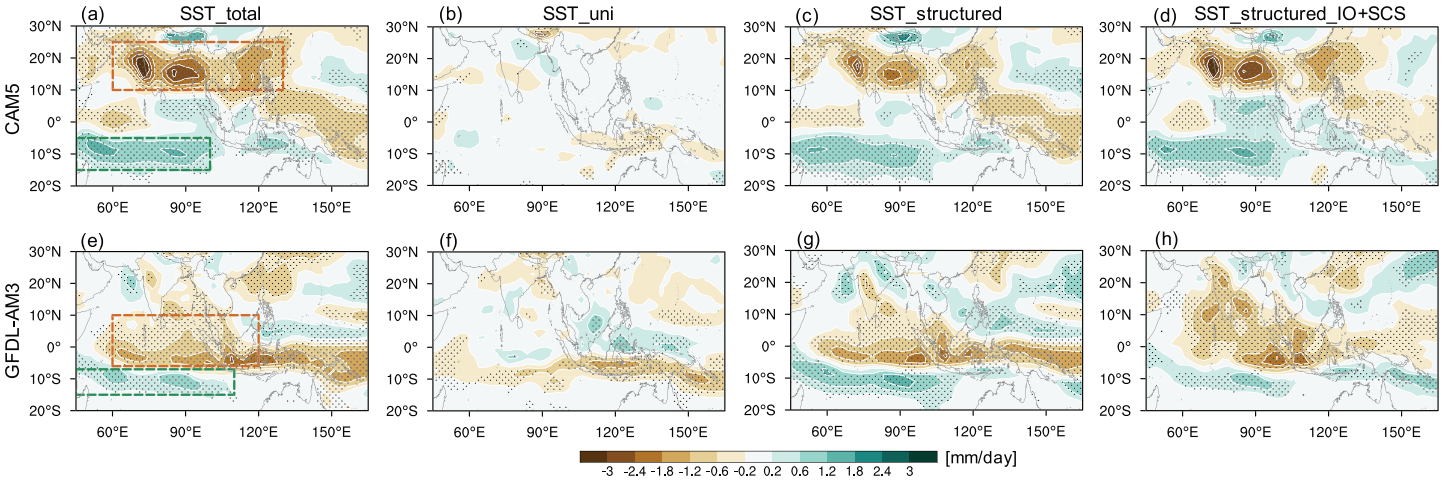

Figure 2. Rainfall (in mm/day) responses from the AGCM experiments with the various SST configurations for CAM5 (top) and GFDL-AM3 (bottom). (a, e) Total aerosol-forced SST, (b, f) uniform cooling part of the SST, (c, g) spatially nonuniform but global SST pattern, and (d, h) nonuniform SST pattern over the Indian Ocean plus South and East China Seas (IO + CSs). Stippling indicates statistical significance at the 5% level using a two-tailed Student's *t* test.

SST experiment. When CSs SST is excluded, the precipitation responses are similar in spatial pattern but about half the magnitude as the one with CSs SST. The presence of the CSs SST cooling (see Figure S1) provides a local north-south SST gradient, which may have dominated the response to global zonal-mean SST gradient in Wang et al. (2019).

We use atmospheric moisture budget analysis to determine the contribution of the thermodynamic and dynamic processes to the monsoon rainfall changes. Figure 3 shows the precipitation (δP), evaporation (δE), δ(P-E), the total mean MC (δMC), as well as the associated thermodynamic (δTH) and dynamic (δDY) contributions to the meridional rainfall dipole shown in Figures 2a and 2e (shown as the difference between the averaged values in the green and red boxes). The spatial distributions of these moisture budget terms are shown in Figures S2 and S3 for CAM5 and GFDL-AM3, respectively. In the South Asian monsoon region, the change in precipitation is balanced by the mean MC, with evaporation contributing little to the balance and a minor role by the transient eddy MC (difference between total δMC and δ(P-E)). As shown in Figure 2, the dipole rainfall changes are predominantly driven by the spatially structured SST in both models. The uniform cooling contributes little to the total MC, and the dynamical and thermodynamical components across both models. This contrasts with the uniform warming of GHG-forced SST (e.g., Li & Ting, 2017) where the thermodynamic contribution due to uniform warming to increasing monsoon rainfall is an important factor. The discrepancy may be due to the magnitude of the warming (4 K in Li & Ting, 2017) being much stronger than the aerosol cooling here, and to a lesser extent the nonlinearity of the Clausius-Clapeyron relationship, where warming will cause more changes in atmospheric moistening than the drying due to cooling. Taken all together, the monsoon rainfall dipole is primarily driven by the spatially structured SST, dominated by the dynamical changes due to atmospheric circulation. Furthermore, this rainfall and circulation change is largely forced by the spatially structured SST changes in the local ocean basins, i.e., IO-CSs (green bars).

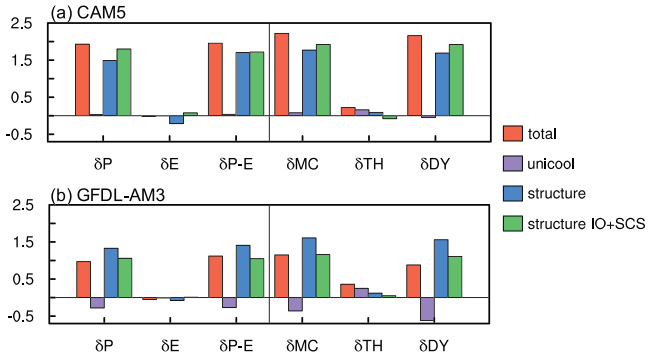

Figure 3. Difference between the green and red boxed regions (in mm/day) for the AGCM's responses to different configurations of the SST (different colors) for precipitation (δ*P*), evaporation (δ*E*), Precipitation minus evaporation (δ*(P − E)*), mean moisture convergence (δ*MC*), thermodynamic (δ*TH*), and dynamic (δ*DY*) component of the mean moisture convergence, for (a) CAM5 and (b) GFDM-AM3.

To further examine the circulation changes, Figure 4 depicts the response of JJA 850 hPa wind vectors to the various SST forcing for the two models. Driven by the total SSTA, both models suggest an overall weakened cross-equatorial flow, thereby reducing the climatological moisture supply to the south Asian region (Figures 4a and 4e) and subsequently reduction in rainfall. Consistent with the rainfall changes shown in Figure 2, there is a meridional shift in the monsoon circulation change, with CAM5 showing a further northward reduction of the monsoon flow opposing

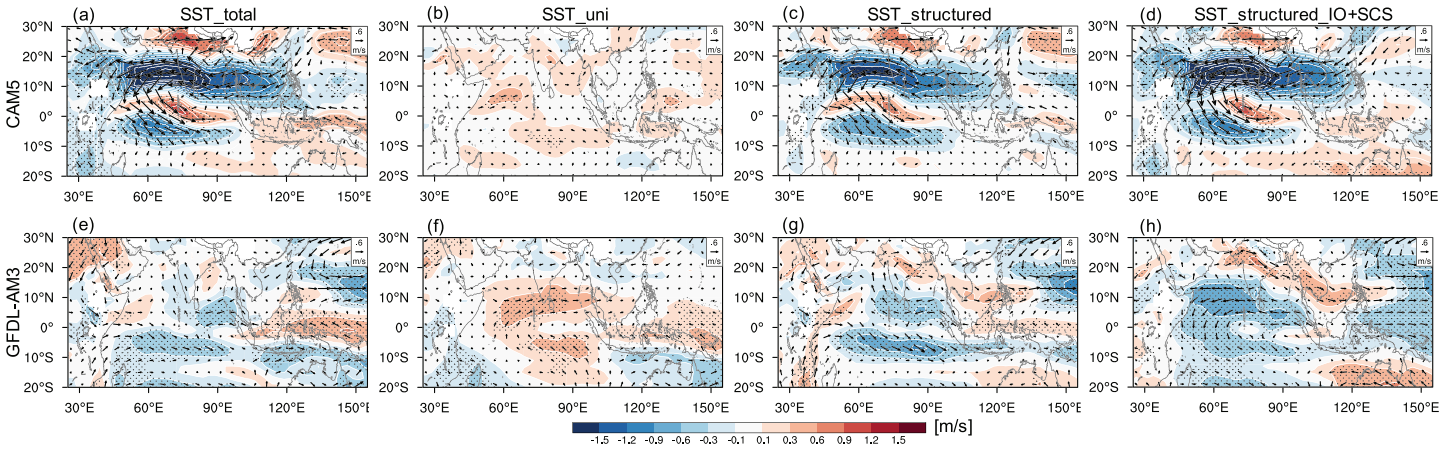

Figure 4. AGCM's 850 hPa wind response in the various SST experiments for CAM5 (top) and GFDL-AM3 (bottom). (a, e) Total aerosol-forced SST, (b, f) uniform cooling part of the SST, (c, g) spatially nonuniform but global SST pattern, and (d, h) nonuniform SST pattern over the Indian Ocean plus South and East China Seas. Stippling indicates statistical significance at the 5% level using a two-tailed Student's *t* test. Arrows show anomalous wind vectors and color shadings show anomalous wind speed in m/s.

directly the climatological winds, whereas GFDL-AM3 shows a weaker and southward shifted reduction in monsoon flow compared to the climatological winds. It is not clear whether the intermodel difference is caused by differences in SST or monsoon climatology. We compared the 850 hPa winds and monsoon rainfall in the control experiments to European Centre for Medium-Range Weather Forecasts (ECMWF) interim reanalysis (ERA-I) winds and Global Precipitation Climatology Project (GPCP) and the Climate Prediction Center Merged Analysis of Precipitation (CMAP) rainfall for the period from 1979 to 2018 in Figure S4. Both models capture the gross features of the observed cross-equatorial monsoon flows, but monsoon rainfall shows substantial discrepancies between models and observations. The pattern correlation with the GPCP (CMAP) rainfall over the domain 40–150°E, 20°S–35°N is 0.46 (0.54) for CAM5 and 0.57 (0.63) for GFDL-AM3. However, the two models do not seem to be substantially different in their ability to capture the observed climatological monsoon circulation and rainfall patterns.

The wind responses resulting from the uniform and structured SSTs are generally opposite to each other in spatial pattern; the uniform SST cooling leads to a slightly enhanced cross-equatorial flow (Figures 4b and 4f) while the structured SST produces a weakened monsoon flow (Figures 4c and 4g) as in the case with total SST. The weakening is further reproduced by the local SST in IO-CSs (Figures 4d and 4h). The slight strengthening of monsoon circulation due to uniform SST cooling is in agreement with the thermodynamic argument for uniform warming, in that the tropical circulation has to weaken to balance the faster increasing rate of atmospheric water vapor (7% K^{-1}) compared to precipitation (2–3% K^{-1}) (Held & Soden, 2006).

The weakening of the monsoon circulation due to structured SST, particularly local SST, is consistent with the energy transport argument. Due to the predominant cooling in the NH, the local meridional overturning circulation, with rising branch in the monsoon region from equator to 30°N and sinking branch at 30°S (see Figure 5 contours, also Figure S5), will weaken in order to reduce the energy transport from NH to SH to offset the aerosol-induced NH cooling. The Asian monsoon overturning circulation and its change are shown in Figure 5, which are illustrated by the local zonal-mean meridional mass streamfunction and rainfall averaged over 40–150°E. The results are insensitive to the exact longitudinal extent of the averaging. While the two AGCMs are capable of reproducing the climatological cross-equatorial cell featuring the expansion of the summer monsoon circulation (Figure S5), the strength seems slightly stronger in both models than in observations. However, the vertical motion associated with the overturning indicates a well captured sinking branch at 30°S and a broad region of monsoon rising motion between equator and 30°N in both models. The aerosol-forced SST in both models tends to weaken the climatological cell. However, the magnitude of the weakening differs, with a much stronger and northward located anomalous cell in CAM5, versus a weaker and more confined reduction in GFDL-AM3. To explore the causes of the different magnitude and latitudinal locations of the two models' circulation responses, we conducted a sensitivity experiment using CAM5 by prescribing GFDL-CM3 IO-CSs SSTA instead. The results are shown in the

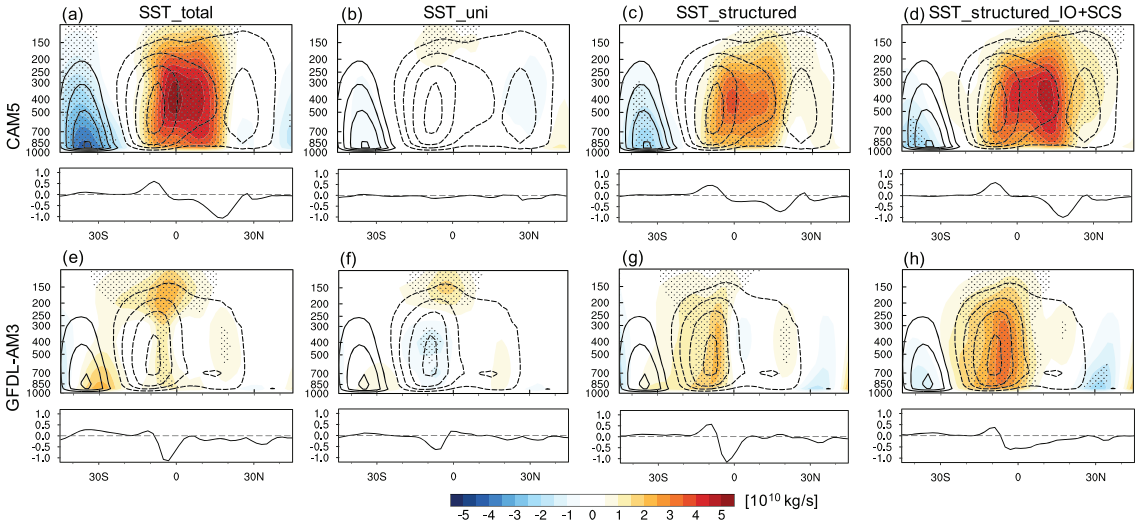

Figure 5. Climatology (contours) and anomalous (shading) meridional mass streamfunction (kg/s) computed for the zonal domain 40°E and 150°E, and longitudinally averaged rainfall anomaly (line plot, in mm/day) for the domain 40–150°E in different SST experiments for CAM5 (top) and GFDL-AM3 (bottom). (a, e) Total aerosol-forced SST, (b, f) uniform cooling part of the SST, (c, g) spatially nonuniform but global SST pattern, and (d, h) nonuniform SST pattern over the Indian Ocean plus South and East China Seas. Stippling indicates statistical significance at the 5% level using a two-tailed Student's *t* test. Contour interval for the climatological mass streamfunction is 10×10^{10} kg/s and dashed contours denote negative values (zero contours are omitted).

middle panels of Figure S6 for precipitation, 850 hPa winds, and meridional mass streamfunction, along with that from CAM5 with CAM5 SST (left) and GFDL-AM3 with GFDL SST (right) for comparison. Figure S6 clearly shows that the intermodel difference is caused by the different SSTA. Even though the GFDL-CM3 produces an aerosol-forced SSTA that is stronger than the corresponding one in the CESM-CAM5, the monsoon response is actually weaker when forced by the stronger SST. Additional experiments with zonally averaged SST in the IO-CSs region showed that it is the location of the strong meridional SST gradient that contributes more to the monsoon circulation response than the amplitude of the SST. The CESM-CAM5 SST (Figure S1a) place the largest SST gradient close to the equator, whereas the largest SST gradient in GFDL-CM3 is near 10°S, leading to the different monsoon circulation response and associated precipitation.

4. Conclusions

Using two comprehensive AGCMs (CAM5 and GFDL-AM3) with prescribed aerosol-forced SSTs taken from the corresponding coupled models, we have investigated the response of the Asian monsoon rainfall and circulation to SSTA induced by anthropogenic aerosols. The total SST change is separated into a uniform cooling and a spatially varying component characterized by interhemispheric temperature contrast. The monsoon rainfall response is dominated by the spatially structured SSTA, especially local SSTA in the IO-CSs, via changes in atmospheric circulation. The weakened meridional temperature gradient due to northern hemisphere centric anthropogenic aerosol forcing leads to weakened monsoon circulation, which drives a dry north-wet south dipole pattern in rainfall change. However, the two models show significant discrepancy in the latitudinal location of the northern drying center and the strength of the monsoon overturning circulation change. These intermodel differences are further shown to be caused by the local SST differences between the two models, particularly the latitudinal location of the SST gradient.

Our results are consistent with earlier studies (Li et al., 2018) that identify the fast and slow responses of South Asian monsoon to aerosol forcing as corresponding to a northern cell and a southern cell, respectively. The southern cell due to the SST forcing places suppressed rainfall slightly north of the equator and enhanced rainfall in the Indian Ocean at around 20°S. But this study further identifies the local SSTA, rather than the global SST pattern induced by aerosol forcing, to be the primary driver of the slow monsoon response to aerosols. Although the two models we employed showed discrepancies in the latitudinal location and strength of the slow responses, the local SSTA as the primary cause of the monsoon slow response is robust across the two models. CAM5 tends to favor a strong and northward shifted overturning monsoon

cell and rainfall response that places suppressed rainfall over the South Asian region. GFDL-AM3 produces a stronger aerosol-induced SST change overall, but a weaker rainfall response in South Asia due to the weaker and southward shifted circulation response, due to the SST gradient being located further south of the rising branch of the local Hadley cell. Our results suggest that model uncertainties in monsoon response to aerosol may be more sensitive to the spatial structure of local SST change due to aerosol forcing.

Acknowledgments
The authors would like to thank Michela Biasutti, Arlene Fiore, and Yochanan Kushnir for comments and discussions. We would also like to thank the two anonymous reviewers for their helpful comments that led to more clarity of the results. We acknowledge support from the National Science Foundation grant AGS16-07348. XL was supported by National Aeronautics and Space Administration (NASA) Headquarters under the NASA Earth and Space Science Fellowship Program grant NNX15AP01H. The CESM project is supported by the National Science Foundation and the Office of Science (BER) of the U.S. Department of Energy. Computing resources were provided by the Climate Simulation Laboratory at NCAR's Computational and Information Systems Laboratory (CISL), sponsored by the National Science Foundation and other agencies. Data generated by this study are available through the IRI/LDEO Climate Data Library (http://kage.ldeo.columbia.edu:81/SOURCES/.LDEO/.ClimateGroup/.PROJECTS/.PublicationsData/.Li_etal_GRL_2019).

References

Allen, M. R., & Ingram, W. J. (2002). Constraints on future changes in climate and the hydrologic cycle. *Nature*, *419*(6903), 228–232. https://doi.org/10.1038/nature01092

Allen, R. J. (2015). A 21st century northward tropical precipitation shift caused by future anthropogenic aerosol reductions. *Journal of Geophysical Research: Atmospheres*, *120*, 9087–9102. https://doi.org/10.1002/2015JD023623

Andrews, T., Forster, P. M., & Gregory, J. M. (2009). A surface energy perspective on climate change. *Journal of Climate*, *22*(10), 2557–2570. https://doi.org/10.1175/2008JCLI2759.1

Bollasina, M. A., Ming, Y., & Ramaswamy, V. (2011). Anthropogenic aerosols and the weakening of the South Asian summer monsoon. *Science*, *334*(6055), 502–505. https://doi.org/10.1126/science.1204994

Bony, S., Bellon, G., Klocke, D., Sherwood, S., Fermepin, S., & Denvil, S. (2013). Robust direct effect of carbon dioxide on tropical circulation and regional precipitation. *Nature Geoscience*, *6*(6), 447–451. https://doi.org/10.1038/NGEO1799

Chadwick, R., Boutle, I., & Martin, G. (2013). Spatial patterns of precipitation change in CMIP5: Why the rich do not get richer in the tropics. *Journal of Climate*, *26*(11), 3803–3822. https://doi.org/10.1175/JCLI-D-12-00543.1

Chen, X., & Zhou, T. (2015). Distinct effects of global mean warming and regional sea surface warming pattern on projected uncertainty in the south Asian summer monsoon. *Geophysical Research Letters*, *42*, 9433–9439. https://doi.org/10.1002/2015GL066384

Donner, L. J., Wyman, B. L., Hemler, R. S., Horowitz, L. W., Ming, Y., Zhao, M., et al. (2011). The dynamical core, physical parameterizations, and basic simulation characteristics of the atmospheric component AM3 of the GFDL global coupled model CM3. *Journal of Climate*, *24*(13), 3484–3519. https://doi.org/10.1175/2011JCLI3955.1

Ganguly, D., Rasch, P. J., Wang, H., & Yoon, J.-H. (2012). Fast and slow responses of the South Asian monsoon system to anthropogenic aerosols. *Geophysical Research Letters*, *39*, L18804. https://doi.org/10.1029/2012GL053043

He, J., & Soden, B. J. (2015). Anthropogenic weakening of the tropical circulation: The relative roles of direct CO_2 forcing and sea surface temperature change. *Journal of Climate*, *28*(22), 8728–8742. https://doi.org/10.1175/JCLI-D-15-0205.1

He, J., Soden, B. J., & Kirtman, B. (2014). The robustness of the atmospheric circulation and precipitation response to future anthropogenic surface warming. *Geophysical Research Letters*, *41*, 2614–2622. https://doi.org/10.1002/2014GL059435

Held, I. M., & Soden, B. J. (2006). Robust responses of the hydrological cycle to global warming. *Journal of Climate*, *19*(21), 5686–5699. https://doi.org/10.1175/JCLI3990.1

Hill, S. A., Ming, Y., & Held, I. M. (2015). Mechanisms of forced tropical meridional energy flux change. *Journal of Climate*, *28*(5), 1725–1742. https://doi.org/10.1175/JCLI-D-14-00165.1

Kang, S. M., Held, I. M., Frierson, D. M. W., & Zhao, M. (2008). The response of the ITCZ to extratropical thermal forcing: Idealized slab-ocean experiments with a GCM. *Journal of Climate*, *21*(14), 3521–3532. https://doi.org/10.1175/2007JCLI2146.1

Kent, C., Chadwick, R., & Rowell, D. P. (2015). Understanding uncertainties in future projections of seasonal tropical precipitation. *Journal of Climate*, *28*(11), 4390–4413. https://doi.org/10.1175/JCLI-D-14-00613.1

Kim, M. J., Yeh, S.-W., & Park, R. J. (2016). Effects of sulfate aerosol forcing on East Asian summer monsoon for 1985–2010. *Geophysical Research Letters*, *43*, 1364–1372. https://doi.org/10.1002/2015GL067124

Lau, W. K.-M., & Kim, K.-M. (2017). Competing influences of greenhouse warming and aerosols on Asian summer monsoon circulation and rainfall. Asia-Pacific. *Journal of the Atmospheric Sciences*, *53*(2), 181–194. https://doi.org/10.1007/s13143-017-0033-4

Li, X., & Ting, M. (2015). Recent and future changes in the Asian monsoon-ENSO relationship: Natural or forced? *Geophysical Research Letters*, *42*, 3502–3512. https://doi.org/10.1002/2015GL063557

Li, X., & Ting, M. (2017). Understanding the Asian summer monsoon response to greenhouse warming: The relative roles of direct radiative forcing and sea surface temperature change. *Climate Dynamics*, *49*(7–8), 2863–2880. https://doi.org/10.1007/s00382-016-3470-3

Li, X., Ting, M., & Lee, D. E. (2018). Fast adjustments of the Asian summer monsoon to anthropogenic aerosols. *Geophysical Research Letters*, *45*, 1001–1010. https://doi.org/10.1002/2017GL076667

Li, X., Ting, M., Li, C., & Henderson, N. (2015). Mechanisms of Asian summer monsoon changes in response to anthropogenic forcing in CMIP5 models. *Journal of Climate*, *28*(10), 4107–4125. https://doi.org/10.1175/JCLI-D-14-00559.1

Liu, L., Shawki, D., Voulgarakis, A., Kasoar, M., Samset, B. H., Myhre, G., et al. (2018). A PDRMIP multimodel study on the impacts of regional aerosol forcings on global and regional precipitation. *Journal of Climate*, *31*(11), 4429–4447. https://doi.org/10.1175/JCLI-D-17-0439.1

Ma, J., & Xie, S.-P. (2013). Regional patterns of sea surface temperature change: A source of uncertainty in future projections of precipitation and atmospheric circulation. *Journal of Climate*, *26*(8), 2482–2501. https://doi.org/10.1175/JCLI-D-12-00283.1

Ming, Y., & Ramaswamy, V. (2009). Nonlinear climate and hydrological responses to aerosol effects. *Journal of Climate*, *22*(6), 1329–1339. https://doi.org/10.1175/2008JCLI2362.1

Ming, Y., & Ramaswamy, V. (2011). A model investigation of aerosol-induced changes in tropical circulation. *Journal of Climate*, *24*(19), 5125–5133. https://doi.org/10.1175/2011JCLI4108.1

Neale, R. B., Andrew Gettelman, Sungsu Park, Andrew J. Conley, Doug Kinnison, Dan Marsh, et al., Microscale Meteorology (2012). Description of the NCAR Community Atmosphere Model (CAM 5.0). Tech. Rep. NCAR/TN-486+STR, National Center for Atmospheric Research (NCAR), Boulder, CO.

Richardson, T. B., Forster, P. M., Andrews, T., & Parker, D. J. (2016). Understanding the rapid precipitation response to CO_2 and aerosol forcing on a regional scale. *Journal of Climate*, *29*(2), 583–594. https://doi.org/10.1175/JCLI-D-15-0174.1

Samset, B. H., Myhre, G., Forster, P. M., Hodnebrog, Ø., Andrews, T., Faluvegi, G., et al. (2016). Fast and slow precipitation responses to individual climate forcers: A PDRMIP multimodel study. *Geophysical Research Letters*, *43*, 2782–2791. https://doi.org/10.1002/2016GL068064

Seager, R., & Henderson, N. (2013). Diagnostic computation of moisture budgets in the ERA-Interim reanalysis with reference to analysis of CMIP-archived atmospheric model data. *Journal of Climate*, *26*(20), 7876–7901. https://doi.org/10.1175/JCLI-D-13-00018.1

Seo, J., Kang, S. M., & Frierson, D. M. W. (2014). Sensitivity of intertropical convergence zone movement to the latitudinal position of thermal forcing. *Journal of Climate*, *27*(8), 3035–3042. https://doi.org/10.1175/JCLI-D-13-00691.1

Shaw, T. A., & Voigt, A. (2015). Tug of war on summertime circulation between radiative forcing and sea surface warming. *Nature Geoscience*, *8*(7), 560–566. https://doi.org/10.1038/ngeo2449

Shindell, D. T., Lamarque, J. F., Schulz, M., Flanner, M., Jiao, C., Chin, M., et al. (2013). Radiative forcing in the ACCMIP historical and future climate simulations. *Atmospheric Chemistry and Physics*, *13*(6), 2939–2974. https://doi.org/10.5194/acp-13-2939-2013

Singh, D. (2016). South Asian monsoon: Tug of war on rainfall changes. *Nature Climate Change*, *6*(1), 20–22. https://doi.org/10.1038/nclimate2901

Turner, A. G., & Annamalai, H. (2012). Climate change and the South Asian summer monsoon. *Nature Climate Change*, *2*(8), 587–595. https://doi.org/10.1038/nclimate1495

Wang, H., Xie, S.-P., Kosaka, Y., Liu, Q., & Du, Y. (2019). Dynamics of Asian summer monsoon response to anthropogenic aerosol forcing. *Journal of Climate*, *32*(3), 843–858. https://doi.org/10.1175/JCLI-D-18-0386.1

Wang, Y., Ma, P.-L., Jiang, J. H., Su, H., & Rasch, P. J. (2016). Toward reconciling the influence of atmospheric aerosols and greenhouse gases on light precipitation changes in eastern china. *Journal of Geophysical Research: Atmospheres*, *121*, 5878–5887. https://doi.org/10.1002/2016JD024845

Westervelt, D. M., Conley, A. J., Fiore, A. M., Lamarque, J. F., Shindell, D., Previdi, M., et al. (2017). Multimodel precipitation responses to removal of U.S. sulfur dioxide emissions. *Journal of Geophysical Research: Atmospheres*, *122*, 5024–5038. https://doi.org/10.1002/2017JD026756

Westervelt, D. M., Conley, A. J., Fiore, A. M., Lamarque, J. F., Shindell, D. T., Previdi, M., et al. (2018). Connecting regional aerosol emissions reductions to local and remote precipitation responses. *Atmospheric Chemistry and Physics*, *18*(16), 12,461–12,475. https://doi.org/10.5194/acp-18-12461-2018

Xie, S.-P., Deser, C., Vecchi, G. A., Collins, M., Delworth, T. L., Hall, A., et al. (2015). Towards predictive understanding of regional climate change. *Nature Climate Change*, *5*(10), 921–930. https://doi.org/10.1038/nclimate2689

Xie, S.-P., Lu, B., & Xiang, B. (2013). Similar spatial patterns of climate responses to aerosol and greenhouse gas changes. *Nature Geoscience*, *6*(10), 828–832. https://doi.org/10.1038/ngeo1931